L-Cysteine-Assisted Synthesis of Layered MoS_2/Graphene Composites with Excellent Electrochemical Performances for Lithium Ion Batteries

Kun Chang and Weixiang Chen*

Department of Chemistry, Zhejiang University, Hangzhou 310027, People's Republic of China

ABSTRACT A facile process was developed to synthesize layered MoS_2/graphene (MoS_2/G) composites by an L-cysteine-assisted solution-phase method, in which sodium molybdate, as-prepared graphene oxide (GO), and L-cysteine were used as starting materials. As-prepared MoS_2/G was then fabricated into layered MoS_2/G composites after annealing in a H_2/N_2 atmosphere at 800 °C for 2 h. The samples were systematically investigated by X-ray diffraction, field emission scanning electron microscopy, energy dispersive X-ray spectroscopy, and high-resolution transmission electron microscopy. Electrochemical performances were evaluated in two-electrode cells *versus* metallic lithium. It is demonstrated that the obtained MoS_2/G composites show three-dimensional architecture and excellent electrochemical performances as anode materials for Li-ion batteries. The MoS_2/G composite with a Mo:C molar ratio of 1:2 exhibits the highest specific capacity of ~1100 mAh/g at a current of 100 mA/g, as well as excellent cycling stability and high-rate capability. The superior electrochemical performances of MoS_2/G composites as Li-ion battery anodes are attributed to their robust composite structure and the synergistic effects between layered MoS_2 and graphene.

KEYWORDS: L-cysteine-assisted · MoS_2/graphene composites · anode material · lithium ion battery · ac impedance

Lithium ion batteries (LIBs) have now become the main power sources for portable electronic devices. They have also attracted extensive attention as power sources for high-power tools and electric vehicles. For an anode material in LIB, the graphitic materials are extensively spread as commercial anode materials because of their flat potential profile *versus* lithium and their structural stability during cycling. However, the small theoretical specific capacity of graphite (372 mAh/g) necessitates the determination of alternative negative electrodes.[1,2] Graphene, a flat, one-atom-thick monolayer exfoliated from graphite, exhibits excellent electronic behavior and mechanical properties, as well as a large specific surface area, so that it has attracted considerable research interest for many applications.[3−5] In particular, graphene nanosheets and their composites have been intensively investigated for their electrochemical properties to determine their suitability as anode materials for LIBs.[6−8] High capacities from ~600 to 1000 mAh/g have been observed for graphene nanosheets and their composites. To date, numerous studies on metal and metal oxides supported on graphene have been conducted, in which their electrochemical performance as anode materials for LIBs was considerably enhanced.[9,10] However, research on layered metal sulfides supported on graphene as LIB anode materials has hardly been reported thus far.

As a typical layered transition metal sulfide, MoS_2 has the analogous structure of graphene; this structure is composed of three stacked atom layers (S−Mo−S) held together by van der Waals forces.[11,12] This layered structure enables the convenient intercalation and exfoliation of Li^+ ions. When the first lithium ion battery patent with MoS_2 as the electrode material was published in 1980,[13] a number of different morphologies of MoS_2 used in LIBs were observed. Feng *et al.*[14] synthesized MoS_2 nanoflakes by a hydrothermal method and found that the MoS_2 nanoflake electrodes exhibit a high insertion capacity of ~1000 mAh/g. In our previous work,[15] nanoflower MoS_2 was also synthesized by ionic liquid-assisted hydrothermal reaction. The nanoflower MoS_2 delivered a reversible capacity of ~900 mAh/g, but their cyclic stability was unsatisfactory and required improvement.

Biomolecular-assisted synthetic methods have recently become the new focus of nanomaterial preparation. Among the numerous biomolecules, L-cysteine (L-cys, $HSCH_2CHNH_2COOH$) is of particular interest to scholars due to its multifunctional groups (−SH, $-NH_2$, and $-COO^-$),[16,17] which can be used for the conjugation of metallic ions

* Address correspondence to weixiangchen@zju.edu.cn.

Received for review February 17, 2011 and accepted May 16, 2011.

Published online May 16, 2011
10.1021/nn200659w

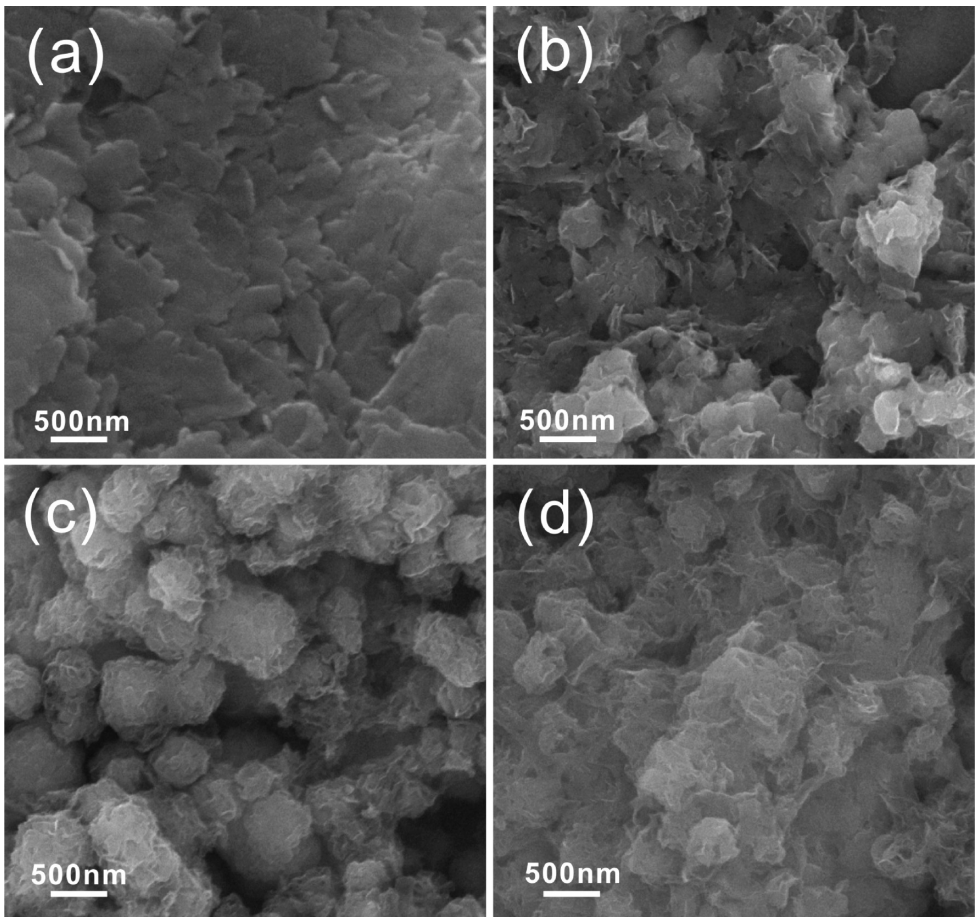

Figure 1. SEM images of (a) MoS_2, (b) MoS_2/G (1:1), (c) MoS_2/G (1:2), and (d) MoS_2/G (1:4) prepared by hydrothermal route and annealing in H_2/N_2 at 800 °C for 2 h.

or other functional groups.[18] When heated, L-cys can release H_2S, which acts a sulfide source as well as a reducing agent, resulting in the formation of metal sulfide nanoparticles. Chen *et al.*[19,20] synthesized a three-dimensional (3D) flower-like β-In_2S_3 by hydrothermal methods using indium chloride and L-cys as starting materials; they found that solution pH, In^{3+} to L-cys molar ratio, and reaction temperature play important roles in the entire process. In our previous work, we successfully synthesized two-dimensional SnS_2/SnO_2 nanoplates *via* an L-cys-assisted method.[21] Under the solution-phase reaction, L-cys formed a polymeric network structure, which facilitated the formation of a two-dimensional structure for the compounds. These layered structural compounds could extensively improve the cycling behavior of the nanoplates in LIBs.

In the present work, we present a facile process for the synthesis of layered MoS_2/graphene (MoS_2/G) composites by an L-cys-assisted solution-phase method, in which sodium molybdate, as-prepared graphene oxide (GO), and L-cys were used as starting materials. The as-prepared MoS_2/G were then fabricated into MoS_2/G composites after annealing in H_2/N_2 atmosphere at 800 °C. The MoS_2/G composites were well characterized by XRD, TEM, HRTEM, and EDAX. The effects of the graphene on the microstructures and electrochemical performances of the composites as Li-ion battery anodes were systematically investigated. It was found that the incorporation of the graphene considerably inhibits the growth of MoS_2 crystals in the composites, especially in the (002) plane of MoS_2 during hydrothermal processing and annealing. The layered MoS_2/G composites exhibited high reversible capacity (up to ~1100 mAh/g) with excellent cyclic stability and high-rate capability.

RESULTS AND DISCUSSION

Characterization of Morphology and Structure. Figure 1 shows a general view of the morphologies of MoS_2, MoS_2/G (1:1), MoS_2/G (1:2), and MoS_2/G (1:4) that were synthesized by hydrothermal method and annealing in a H_2/N_2 atmosphere at 800 °C for 2 h. As shown in Figure 1a, the bare MoS_2 obtained through the proposed method consists of large-scale sheets that are tightly stacked together. When GO was predispersed in hydrothermal solution, the synthesized MoS_2/G composites display a 3D architecture morphology consisting of nanosheets, as shown in Figure 1c,b,d. In particular, the MoS_2/G (1:2) composite displays a 3D sphere-like architecture (Figure 1c). The 3D architecture

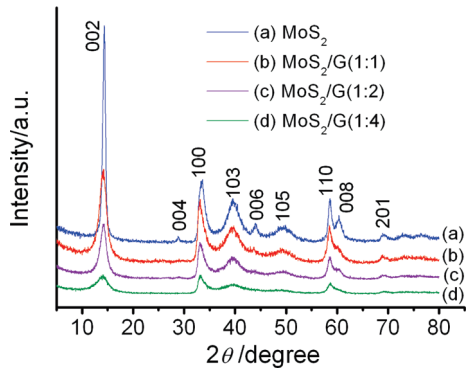

Figure 2. XRD patterns of (a) MoS_2, (b) MoS_2/G (1:1), (c) MoS_2/G (1:2), and (d) MoS_2/G (1:4) prepared by hydrothermal route and annealing in H_2/N_2 at 800 °C for 2 h.

of MoS_2/G composites was attributed to the graphene self-assembling during the hydrothermal process, in which GO was reduced to graphene and the flexible graphene self-assembled into a 3D architecture by partial overlapping or coalescing.[22] 3D morphology of MoS_2/G composites still remained after their annenling.

The XRD patterns of the samples are shown in Figure 2. As shown in Figure 2a, the MoS_2 synthesized by L-cys exhibits high crystallinity and a typical hexagonal structure after annealing in H_2/N_2 at 800 °C, which is in accordance with those established by JCPDS card number 37-1492. Figure 2a shows that the primary (002) diffraction peak appears at 2θ = 14.2° with a *d*-spacing of 0.62 nm, indicating that the layered MoS_2 grows well along the *c* axis during annealing. From Figure 2b,c,d, we also observe that the MoS_2/G composites basically retain the layered crystallinity and the position of the diffraction peaks of MoS_2. However, it is worth noticing that the intensity of all the diffraction peaks of MoS_2 decrease with increasing graphene proportion in the composites, especially the (002) plane peaks, which indicate that the incorporation of the graphene considerably inhibits the (002) plane growth of MoS_2 crystals in the composites. Additionally, the XRD patterns of the MoS_2/G composites show that the (002) diffraction peaks of the graphene nanosheets cannot be detected,[23] indicating that the graphene nanosheets do not stack during the hydrothermal process and annealing. More recently, Li *et al.*[24] demonstrated that the GO nanosheets could be used as a novel substrate for the nucleation and subsequent growth of MoS_2 and found (by microscopy and Raman imaging) that the growth of MoS_2 is selective on GO, with little free particle growth in solution. The selective growth of MoS_2 on GO was attributed to the interaction between the oxygen-containing functional groups on GO sheets and Mo precursors. In our present work, MoO_4^{2-} was reduced to MoS_2 by L-cys, and GO was also *in situ* reduced to graphene by L-cys during the hydrothermal process. In this process, GO or reduced GO could act as a substrate

TABLE 1. Element Composition of Layered MoS_2/G Composites after Annealing in H_2/N_2 at 800 °C for 2 h with Different Graphene Contents

	element (wt %)			
composite	C	O	Mo	S
MoS_2/G (1:1)	5.62	2.67	55.99	35.72
MoS_2/G (1:2)	12.93	3.55	49.99	33.53
MoS_2/G (1:4)	23.65	5.38	42.10	28.87

for the nucleation and growth of MoS_2. Due to the layered MoS_2 growth on GO or reduced GO surface, the stacking of the graphene was inhibited during the hydrothermal process, even during annealing. *Vice versa*, the incorporation of the graphene also restrained the (002) plane growth of MoS_2 crystals in the composites during annealing.

To determine the composition of the samples, we identified the layered MoS_2/G composites from EDAX. The element compositions of the layered MoS_2/G composites with different graphene contents are summarized in Table 1. The table shows that the samples contain C, Mo, S, and a small quantity of O. The calculated atomic ratio of S to Mo element ranges from 1.91 to 2.06, approaching the theoretical value of MoS_2. These values indicate that the products are stoichiometric MoS_2. C is provided by graphene, while a small quantity of O comes from a few parts of the graphene that were not completely reduced during the hydrothermal process and annealing. Table 1 also shows that the Mo:C atomic ratio approaches the theoretical value of the MoS_2/G composites (1:1, 1:2, and 1:4).

Experimental characterization reveals that the MoS_2/G composites deliver a composite structure of layered MoS_2 and graphene after annealing. Subsequently, we analyzed the microstructure of the MoS_2/G (1:2) sample in detail. Figure 3a shows that the micro-sized MoS_2/G (1:2) composite displays a 3D architecture, which is composed of a large number of scaled and curved sheets in the range 100−200 nm. Its 3D architecture is caused by the self-assembly of *in situ* reduced GO into a 3D architecture by the partial overlapping or coalescing of the flexible graphene during the hydrothermal process.[22] 3D architectural MoS_2/G composites as LIB anodes would increase the contact area with the electrolyte and also provide more and shorter Li-ion diffusion channels during the lithiation/delithiation processes. In addition, the overlapping or coalescing of the graphene would form an interconnected conducting network, which is very important for the less-conducting MoS_2 as electrode materials, and facilitate rapid electronic transport in electrode reactions. Finally, this 3D structure also enhances the stability of the MoS_2/G composites due to superstrength of graphene.[25] From Figure 3b, it can be clearly seen that layered MoS_2 is supported on the

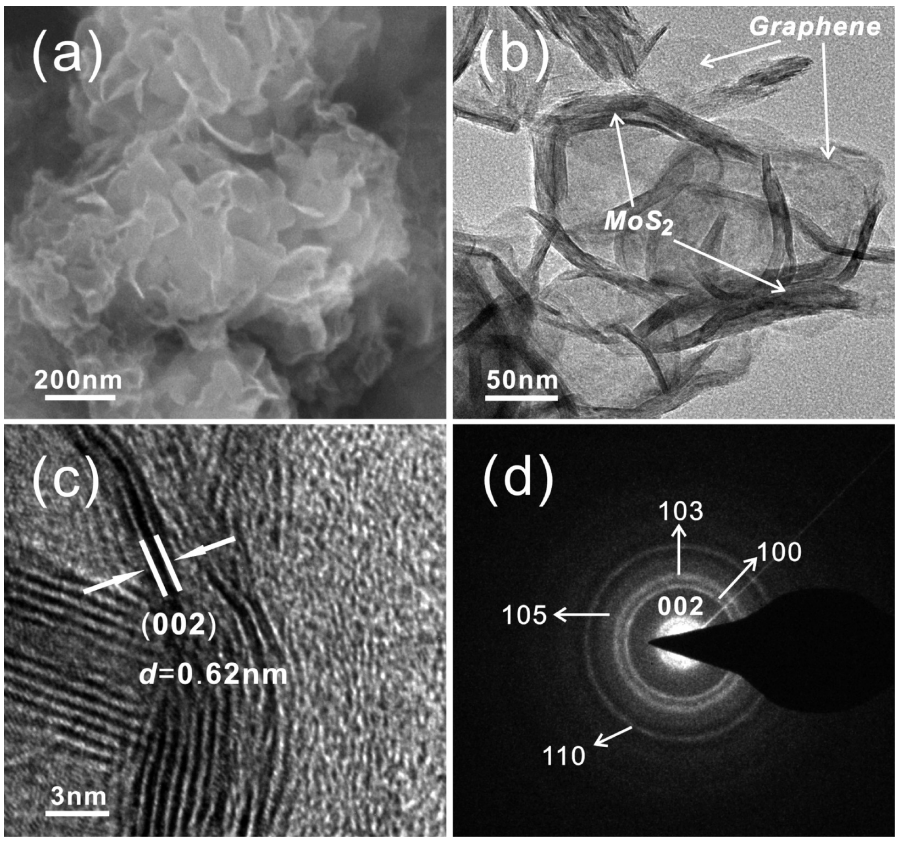

Figure 3. Microstructure of MoS_2/G (1:2) composite: (a) SEM image, (b) TEM image, (c) HRTEM image, and (d) electron diffraction pattern.

graphene surface. The HRTEM image of the MoS_2/G (1:2) in Figure 3c shows the typical layered MoS_2 with a few layers (4−11) and an interlayer distance of 0.62 nm. A selected-area electron diffraction pattern is shown in Figure 3d and is well-indexed as a pure hexagonal MoS_2 phase. This result indicates that the graphene layers reduced by L-cys do not stack together.

Growth Mechanism. Revealing the growth mechanism of MoS_2/G composites during the hydrothermal process requires investigating the microstructure and morphology of the composites before annealing. Figure 4 shows the XRD patterns and SEM images of the as-prepared MoS_2/G composites with different graphene contents. Comparing with Figures 1 and 2, microstructures and morphologies of the composites after annealing, it is found that the morphologies of the composites before and after annealing do not significantly change but the crystalline structure does. As shown in Figure 4a, the as-prepared MoS_2/G composites display only three very weak diffraction peaks, which is attributed to the (002), (100), and (110) planes of MoS_2, indicating the crystallinity of MoS_2 is very poor. The poor crystallinity of MoS_2 is attributed to the incorporation of the graphene inhibiting the growth of the layered MoS_2 crystal during the hydrothermal process. MoO_4^{2-} precursors were reduced to MoS_2 by L-cys, while the GO was also *in situ* reduced to graphene during the hydrothermal process. The reduced GO provided a substrate for the nucleation and growth of MoS_2. Li *et al*. attributed the selective growth of MoS_2 on GO or reduced GO surface to the interaction between functional groups on the GO sheets and Mo precursors.[24] However, reduced GO also disturbed the growth of layered MoS_2 crystals, especially in the (002) plane of MoS_2. Figure 2 also demonstrates that the graphene inhibits the (002) plane growth of MoS_2 crystals in the composites during annealing. L-cys plays a role of reducing agent and sulfur donor during the whole hydrothermal process, in which L-cys released H_2S as a sulfide source as well as a reducing agent, resulting in the reduction of MoO_4^{2-} precursors to MoS_2 and reduction of GO to graphene. On the basis of the common knowledge concerning elemental sulfur and its compounds, the reaction routes for the synthesis of MoS_2 by L-cys could be expressed as follows:[26]

$$HSCH_2CHNH_2COOH + H_2O \rightarrow CH_3COCOOH + NH_3 + H_2S \quad (1)$$

$$4MoO_4^{2-} + 9H_2S + 6CH_3COCOOH \rightarrow 4MoS_2 + SO_4^{2-} + 6CH_3COCOO^- + 12H_2O \quad (2)$$

Figure 4b,c,d also shows that the morphology of the MoS_2/G composites is a 3D architecture. According to the view of Shi *et al*.,[22] self-assembling graphene into

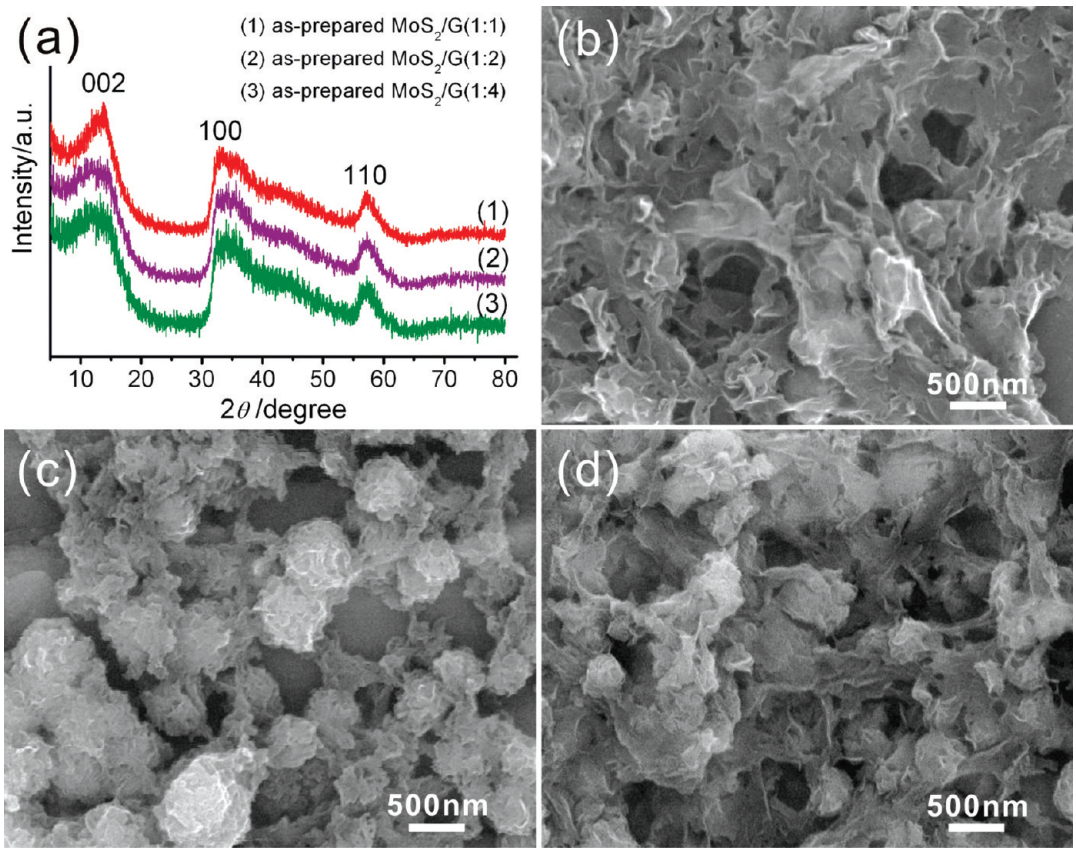

Figure 4. Characterizations of MoS_2/G composites before annealing: (a) XRD patterns of (1) as-prepared MoS_2/G (1:1), (2) as-prepared MoS_2/G (1:2), (3) as-prepared MoS_2/G (1:4), and the SEM images of (b) as-prepared MoS_2/G (1:1), (c) as-prepared MoS_2/G (1:2), and (d) as-prepared MoS_2/G (1:4).

3D macrostructures can be easily presented during the hydrothermal process. Because the partial overlapping or coalescing of flexible graphene resulted in the formation of physical cross-linking sites of the framework of the self-assembled graphene hydrogel, the inherent flexibility of graphene is a crucial property for constructing the 3D structures. Therefore, the MoS_2/G composites display 3D structures due to the self-assembling of the graphene during the hydrothermal process. In particular, as shown in Figure 4c the MoS_2/G (1:2) composite displays a 3D sphere-like morphology, which still remains even after annealing.

Many references indicated that the reduced GO by the chemical method still retained a small amount of oxygen-functionalized groups, such as hydroxyl, carboxyl, and epoxy groups.[27−29] In this work, the as-prepared MoS_2/G composites also contain some of these oxygen-containing functional groups. For determining the composition of samples, the element compositions of the as-prepared MoS_2/G composites were identified by EDAX before annealing, and the results are summarized in Table 2. It can be found from Table 2 that the Mo:S molar ratio is approximate 1.0:2.0, which is in accordance with that in Table 1. However, the contents of O in as-prepared MoS_2/G samples are higher than those of the annealed MoS_2/G composites,

TABLE 2. Element Composition of As-Prepared MoS_2/G Composites before Annealing with Different Contents of Graphene

	element (wt %)			
as-prepared composite	C	O	Mo	S
MoS_2/G (1:1)	6.32	6.23	52.40	35.05
MoS_2/G (1:2)	12.50	7.09	49.71	30.70
MoS_2/G (1:4)	24.92	10.15	38.36	26.57

which is because sections of oxygen-containing functional groups of reduced GO were further reduced during annealing at H_2/N_2.

Electrochemical Performance. Figure 5 shows the first three charge and discharge curves of the annealed MoS_2, MoS_2/G (1:1), MoS_2/G (1:2), and MoS_2/G (1:4) composites at a current density of 100 mA/g. Figure 5a illustrates that two potential plateaus, at 1.1 and 0.6 V, are observed for the annealed MoS_2 electrode in the first discharge (lithiation process). A plateau at 1.1 V is indicative of the formation of Li_xMoS_2, and the plateau variation in the lithium intercalation is attributed to the different defect sites of MoS_2.[30] The plateau at 0.6 V can be attributed to a conversion reaction process, which first entails the *in situ* decomposition of MoS_2 into Mo

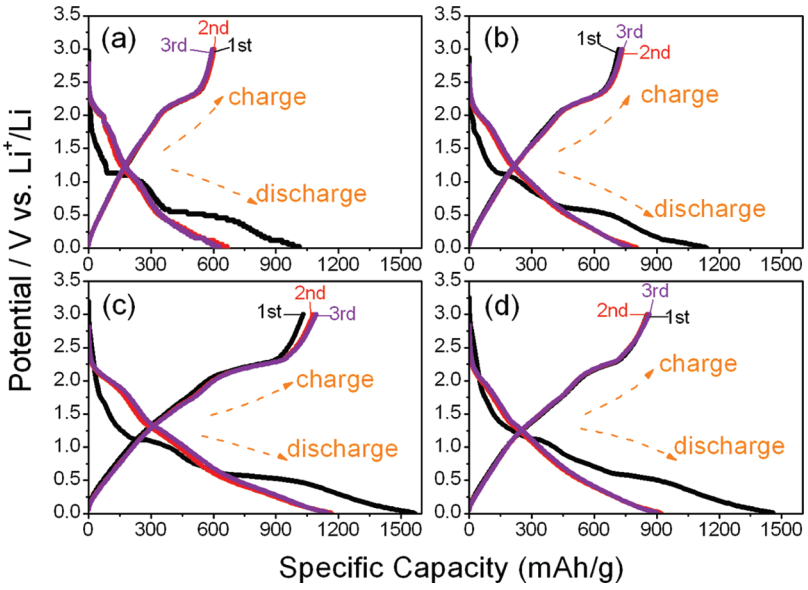

Figure 5. First three charge and discharge curves of the samples after annealing in H_2/N_2 at 800 °C for 2 h at a current density of 100 mA/g in a half-cell composed of MoS_2/G and Li: (a) MoS_2, (b) MoS_2/G (1:1), (c) MoS_2/G (1:2), and (d) MoS_2/G (1:4).

particles embedded into a Li_2S matrix and then the formation of a gel-like polymeric layer resulting from electrochemically driven electrolyte degradation.[31] In the second and third discharge curves, the annealed MoS_2 electrode displays two potential plateaus, at 1.9 and 1.2 V, and the potential plateau at 0.6 V in the first discharge disappears. In the charge (delithiation) process, the annealed MoS_2 electrodes exhibit conspicuous potential plateaus at 2.2 V because of the high crystallinity of the annealed MoS_2. Figure 5b,c shows that the MoS_2/G electrodes display conspicuous potential plateaus at 1.1 and 0.6 V in the first discharge (lithiation) process and at 2.2 V in the first charge (delithiation) process. These results are in accordance with those obtained for the annealed MoS_2. However, for the MoS_2/G (1:4) sample, the potential plateaus become inconspicuous because of the increasing amounts of graphene. The graphene prepared by the chemical method possibly contains a number of amorphous carbons that exhibit stronger disorder and dispersion. As shown in ref 6, pure graphene nanosheets exhibit inconspicuous potential plateaus during charge and discharge processes. Cyclic voltammetry (CV) was performed on the MoS_2 and MoS_2/G (1:2) composite electrodes, whose CV curves are shown in Figure 6. The two samples exhibit peaks at 0.4 and 0.9 V in the first cathodic sweep. The peak at 0.9 V can be attributed to the coordination of Mo by six S atoms (MoS_6), which change from trigonal prisms to octahedra in the MoS_2 structure, whereas lithium ions intercalate into MoS_2, as reported in the literature.[13,31] The peak at 0.4 V is attributed to the conversion reaction process $MoS_2 + 4Li \rightarrow Mo + 2Li_2S$.[32] In the second cathodic sweep, two other peaks, at 1.6 and 2.3 V, appear. However, the peaks located at 0.4 and 0.9 V

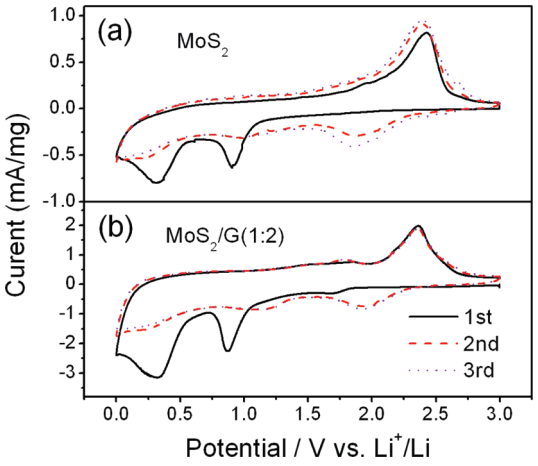

Figure 6. Cyclic voltammograms of (a) MoS_2 and (b) MoS_2/G (1:2) at a scanning rate of 0.5 mV/s during the first three cycles.

disappear—a result that agrees with the previous lithiation and delithiation profiles. During the anodic sweep, both samples exhibit only one peak at 2.4 V, which also agrees with the previous lithiation and delithiation profiles.

Figure 5 illustrates that the initial lithiation (discharge) capacities of the MoS_2, MoS_2/G (1:1), MoS_2/G (1:2), and MoS_2/G (1:4) electrodes are 1012, 1142, 1571, and 1462 mAh/g, respectively, while the initial delithiation (charge) capacities are 600, 718, 1031, and 855 mAh/g, respectively. Among these samples, MoS_2/G (1:2) exhibits the highest lithiation and delithiation capacities. Compared with the theoretical capacity of bulk MoS_2 (only 167 mAh/g),[33] the first discharge capacity of the pristine MoS_2 prepared in the present study exceeds that of bulk MoS_2. The specific capacity of the MoS_2/G composites is greatly

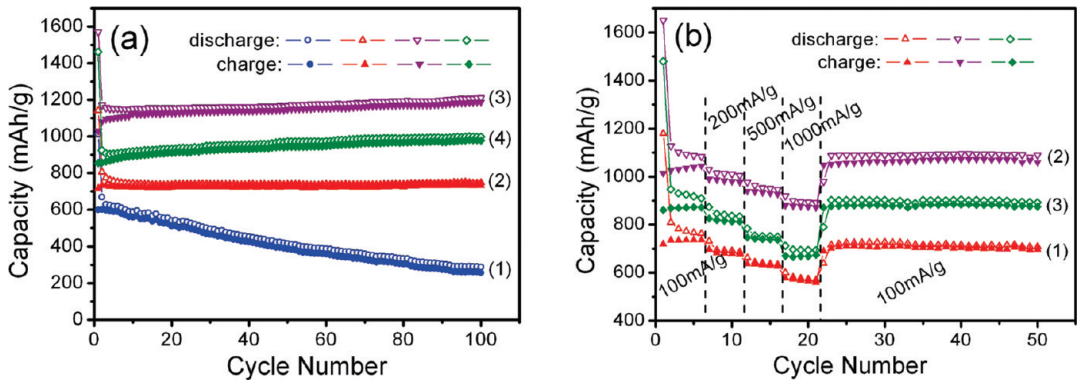

Figure 7. (a) Cycling behavior of samples after annealing in H_2/N_2 at 800 °C for 2 h at a current density of 100 mA/g: (1) MoS_2; (2) MoS_2/G (1:1); (3) MoS_2/G (1:2); (4) MoS_2/G (1:4). (b) Rate capability of MoS_2/G samples at different current densities: (1) MoS_2/G (1:1); (2) MoS_2/G (1:2); (3) MoS_2/G (1:4).

enhanced. As shown in Figure 7a, the cyclic stability of MoS_2 is so poor that the reversible capacity decreases to 256 mAh/g after 100 cycles. This value is only 42.7% of the initial capacity. On the contrary, the MoS_2/G composites exhibit excellent cyclic stabilities. The reversible capacities of the MoS_2/G electrodes do not decrease but slightly increase. After 100 cycles, the reversible capacities of the MoS_2/G (1:1), MoS_2/G (1:2), and MoS_2/G (1:4) electrodes remain at 734, 1187, and 978 mAh/g, respectively. Thus, the incorporation of graphene not only significantly enhances the specific capacities of the composites but also improves their cyclic stabilities due to the robust composite structure and the synergistic effect between the layered MoS_2 and the graphene.

The high reversible capacity and excellent cycling behavior of the MoS_2/G composites are also exhibited in the rate capability. Figure 7b shows the rate cycling behavior of the composites. Among these electrodes, MoS_2/G (1:2) also demonstrates better rate performance. Even at a high current density of 1000 mA/g, the specific capacity remains at ~900 mAh/g, which is still higher than that of MoS_2 at a low current density of 100 mA/g. Additionally, the extraordinary cycling stabilities of the three electrodes are exhibited at various current densities. As shown in Figure 7b, when the charge/dischagrge current density changes from 1000 to 100 mA/g, the specific capacities of the composites return to the last values, which do not immediately change under the current densities and do not ultimately change in the subsequent cycles, indicating extraordinarily high cycling stabilities.

Graphene plays a highly important role in the electrochemical performance of the MoS_2/G composites. The specific capacity of the composites is tremendously enhanced, and their cycling stability and high rate capability are also significantly improved. In order to understand why the MoS_2/G electrode exhibits such a superior electrochemical performance compared to the MoS_2 electrode, ac impedance measurements were performed after 10 cycles, as shown

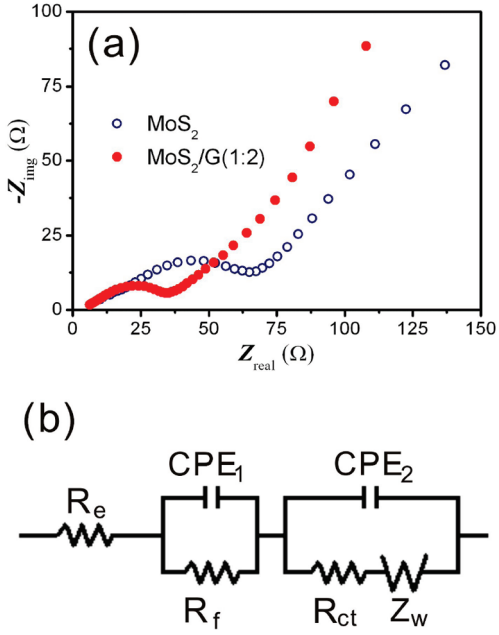

Figure 8. (a) Nyquist plots of MoS_2 and MoS_2/G (1:2) electrodes obtained by applying a sine wave with amplitude of 5.0 mV over the frequency range from 100 kHz to 0.01 Hz; (b) equivalent circuit model of the studied system. CPE represents the constant phase element, $Z_{CPE} = \{Q(j\omega)^n\}^{-1}$, $0 \le n \le 1$.

TABLE 3. Impedance Parameters Derived Using Equivalent Circuit Model for MoS_2 and MoS_2/G (1:2) Electrodes

electrode	R_e (Ω)	R_f (Ω)	Q_1 (μF)	R_{ct} (Ω)	Q_2 (μF)
MoS_2	6.94	13.55	14.5	40.76	45.2
MoS_2/G(1:2)	4.49	8.53	152	13.60	471.3

in Figure 8a. The equivalent circuit model of the studied system is also shown in Figure 8b according to the works reported by others.[34,35] R_e represents the internal resistance of the test battery, R_f and CPE_1 are associated with the resistance and constant phase element of the SEI film, R_{ct} and CPE_2 are associated with the charge-transfer resistance and constant phase

element of the electrode/electrolyte interface, and Z_W is associated with the Warburg impedance corresponding to the lithium-diffusion process. As shown in Figure 8a, the high-frequency semicircle corresponds to the resistance R_f and CPE_1 of the SEI film, and the semicircle in the medium-frequency region is assigned to the charge-transfer resistance R_{ct} and CPE_2 of the electrode/electrolyte interface. The inclined line corresponds to the lithium-diffusion process within the bulk of the electrode material. The kinetic differences of MoS_2/G and bare MoS_2 electrodes were further investigated by modeling ac impendence spectra based on the modified equivalent circuit.[36,37] The fitted impedance parameters are listed in Table 3. It can be seen that the SEI film resistance R_f and charge-transfer resistance R_{ct} of the MoS_2/G (1:2) electrode are 8.53 and 13.60 Ω, which are significantly lower than those of bare MoS_2 (13.55 and 40.76 Ω). This fact confirms that the incorporation of graphene can preserve the high conductivity of the MoS_2/G composite electrode and greatly enhance rapid electron transport during the electrochemical lithium insertion/extraction reaction, resulting in significant improvement in the electrochemical performances. This novel kind of MoS_2/G composites with high reversible capacity, excellent cyclic stability, and high-rate capability would find wide applications as promising anode materials for LIBs.

CONCLUSIONS

A facile process was developed to synthesize layered MoS_2/G composites by an L-cys-assisted solution-phase method and subsequent annealing in a H_2/N_2 atmosphere at 800 °C for 2 h. The characterizations demonstrate that the layered MoS_2 are supported on the graphene surface, which then form the MoS_2/G composites. The addition of graphene would inhibit the growth of layered MoS_2 crystals in the composites, especially in the (002) plane of MoS_2, during the hydrothermal process and annealing. The MoS_2/G composites exhibit a 3D architecture morphology consisting of curved nanosheets, which is attributed to the self-assembling of graphene hydrogel during the hydrothermal process. In particular, the MoS_2/G (1:2) composite delivers a 3D sphere-like architecture. The electrochemical evaluations reveal that all the MoS_2/G composite electrodes exhibit much higher specific capacities and more cyclic stability than bare MoS_2 electrodes. Among the samples, MoS_2/G (1:2) exhibits the highest specific capacity of ~1100 mAh/g at a current density of 100 mA/g and no capacity fading after 100 cycles. Even at a high current density of 1000 mA/g, the specific capacity of MoS_2/G (1:2) remains at ~900 mAh/g with excellent cyclic stability. Alternating current impendence spectra confirm that the incorporation of graphene preserves the high conductivity and greatly enhances the electrochemical activity for the MoS_2/G composites. The excellent electrochemical performances of MoS_2/G composite electrodes are attributed to the robust composite structure and the synergistic effects between layered MoS_2 and graphene. Therefore, the present results suggest that this novel kind of MoS_2/G composite holds great potential as an anode material for LIBs.

EXPERIMENTAL DETAILS

Synthesis of Graphene Oxide. Natural graphite powder (Shanghai Colloid Chemical Plant, China) was oxidized to graphite oxide using a modified Hummers method.[38] Graphite powder was poured into 50 mL of concentrated H_2SO_4 under an ice bath. Then, 3 g of $KMnO_4$ was gradually added. The mixture was stirred for 2 h and then diluted with deionized (DI) water. After that, 10 mL of 30% H_2O_2 was added to the solution until the color of the mixture changed to brilliant yellow. The as-obtained graphite oxide was redispersed in DI water and then exfoliated to generate graphene oxide sheets by ultrasonication. A brown, homogeneous supernatant was obtained by centrifuged washing.

Synthesis of MoS_2/G Composites. GO (prepared by 0.017 g of graphite) was transferred from the as-made suspension into a 200 mL beaker with adding 40 mL of DI water, Then, 0.3 g of $Na_2MoO_4 \cdot 2H_2O$ was added. After ultrasonication and stirring for 20 min, 0.1 M NaOH was added to the solution until the pH value changed to 6.5. The mixture and 0.8 g of L-cysteine were dissolved in 80 mL of DI water and then transferred into a 100 mL Teflon-lined stainless steel autoclave, sealed tightly, and heated at 240 °C for 24 h. After cooling naturally, the black precipitates were collected by centrifugation, washed with DI water and ethanol, and dried in a vacuum oven at 80 °C for 24 h. The composites were annealed in a conventional tube furnace at 800 °C for 2 h in a stream of 10% hydrogen in nitrogen flowing at 200 sccm (standard cubic centimeter per minute). Then the MoS_2/G composites with 1:1 molar ratio of MoS_2 to graphene were obtained and were designated as MoS_2/G (1:1). With the same method as above, MoS_2/G composites with 1:2 (GO was prepared by 0.035 g of graphite) and 1:4 (GO was prepared by 0.065 g of graphite) molar ratios of Mo to C were obtained as well and were designated as MoS_2/G (1:2) and MoS_2/G (1:4), respectively.

Characterizations. The samples were characterized with X-ray diffraction (XRD; Thermo X'TRA X-ray diffractometer with Cu Kα source), high-resolution transmission electron microscopy (HRTEM; JEOL JEM-2010, 200 kV), field emission scanning electron microscopy (FESEM; SIRION-100), and energy dispersive X-ray spectroscopy (EDX, GENENIS-4000).

Electrochemical Measurements. The electrochemical tests were measured using two-electrode cells assembled in an argon-filled glovebox. Li sheets served as the counter electrode and reference electrode, and a polypropylene film (Celgard-2300) was used as a separator. The electrolyte was a 1.0 M $LiPF_6$ solution in a mixture of ethylene carbonate/dimethyl carbonate (EC/DMC) (1:1 in volume). The working electrodes were prepared by a slurry coating procedure. The slurry consisted of 80 wt % active material, 10 wt % acetylene black, and 10 wt % polyvinylidene fluorides dissolved in *N*-methyl-2-pyrrolidinone. This slurry was spread on copper foil, which acted as a current collector. The coated electrodes were dried at 110 °C for 12 h under vacuum and then pressed. Galvanostatic charge/discharge cycles were carried out on a CBT-138-320 battery tester between 0.01 and 3.00 V at various current densities. Cyclic voltammetry measurements were carried out on an electrochemical workstation (Zahner IM6ex) over the potential range

0.01−3.00 V *vs* Li/Li^+ at a scan rate of 0.5 mV/s. Alternating current impendence spectra (PARSTAR 2273) were obtained by applying a sine wave with amplitude of 0.5 mV over the frequency range from 100 kHz to 0.01 Hz.

Acknowledgment. This work was supported by the Zhejiang Provincial Natural Science Foundation of China (Y407030, Y4100119), the Zhejiang Provincial Science and Technology Program for Public Interest (2011C31G2010027), and 973 Fundamental Research Program from the Ministry of Science and Technology of China (2010CB635116).

REFERENCES AND NOTES

1. Tarascon, J. M.; Armand, M. Issues and Challenges Facing Rechargeable Lithium Batteries. *Nature* **2001**, *414*, 359–367.
2. Breger, J.; Meng, Y. S.; Hinuma, Y.; Kumar, S.; Kang, K.; Shao-Horn, Y.; Ceder, G.; Grey, C. P. Effect of High Voltage on the Structure and Electrochemistry of $LiNi_{0.5}Mn_{0.5}O_2$: A Joint Experimental and Theoretical Study. *Chem. Mater.* **2006**, *18*, 4678–4781.
3. Geim, A. K.; Novoselov, K. S. The Rise of Graphene. *Nat. Mater.* **2007**, *6*, 183–191.
4. Yoo, E.; Kim, J.; Hosono, E.; Zhou, H. S.; Kudo, T.; Honma, I. Large Reversible Li Storage of Graphene Nanosheet Families for Use in Rechargeable Lithium Ion Batteries. *Nano Lett.* **2008**, *8*, 2277–2282.
5. Chen, J.; Liu, Y.; Minett, A. I.; Lynam, C.; Wang, J.; Wallace, G. G. Flexible, Aligned Carbon Nanotube/Conducting Polymer Electrodes for a Lithium-ion Battery. *Chem. Mater.* **2007**, *19*, 3595–3597.
6. Wang, G. X.; Shen, X. P.; Yao, J.; Park, J. Graphene Nanosheets for Enhanced Lithium Storage in Lithium Ion Batteries. *Carbon* **2009**, *47*, 2049–2053.
7. Wang, D. H.; Kou, R.; Choi, D. W.; Yang, Z. G.; Nie, Z. M.; Li, J.; Saraf, L. V.; Hu, D. H.; Zhang, J. G.; Graff, G. L.; Liu, J.; Pope, M. A.; Aksay, I. A. Ternary Self-Assembly of Ordered Metal Oxide-Graphene Nanocomposites for Electrochemical Energy Storage. *ACS Nano* **2010**, *4*, 1587–1595.
8. Wang, X. X.; Wang, J. N.; Su, L. F. Preparation and Electrochemical Performance of Ultra-short Carbon Nanotubes. *J. Power Sources* **2009**, *186*, 194–200.
9. Wang, H. L.; Cui, L. F.; Yang, Y.; Casalongue, H. S.; Robinson, J. T.; Liang, Y. Y.; Cui, Y.; Dai, H. J. Mn_3O_4-Graphene Hybrid as a High-Capacity Anode Material for Lithium Ion Batteries. *J. Am. Chem. Soc.* **2010**, *132*, 13978–13980.
10. Wu, Z. S.; Ren, W. C.; Wen, L.; Gao, L. B.; Zhao, J. P.; Chen, Z. P.; Zhou, G. M.; Li, F.; Cheng, H. M. Graphene Anchored with Co_3O_4 Nanoparticles as Anode of Lithium Ion Batteries with Enhanced Reversible Capacity and Cyclic Performance. *ACS Nano* **2010**, *4*, 3187–3194.
11. Tenne, R.; Margulis, L.; Genut, M.; Hodes, G. Polyhedral and Cylindrical Structures of Tungsten Disulfide. *Nature* **1992**, *360*, 444–446.
12. Matte, H. S. S. R.; Gomathi, A.; Manna, A. K.; Late, D. J.; Datta, R.; Pati, S. K.; Rao, C. N. R. MoS_2 and WS_2 Analogues of Graphene. *Angew. Chem., Int. Ed.* **2010**, *49*, 4059–4062.
13. Haering, R. R.; Stiles, J. A. R.; Brandt, K. Lithium Molybdenum Disulphide Battery Cathode. US Patent 4224390, 1980.
14. Feng, C. Q.; Ma, J.; Li, H.; Zeng, R.; Guo, Z. P.; Liu, H. K. Synthesis of Molybdenum Disulfide (MoS_2) for Lithium Ion Battery Applications. *Mater. Res. Bull.* **2009**, *44*, 1811–1815.
15. Li, H.; Li, W. J.; Ma, L.; Chen, W. X.; Wang, J. M. Electrochemical Lithiation/Delithiation Performances of 3D Flowerlike MoS_2 Powders Prepared by Ionic Liquid Assisted Hydrothermal Route. *J. Alloys Compd.* **2009**, *471*, 442–447.
16. Zhang, B.; Ye, X. C.; Hou, W. Y.; Zhao, Y.; Xie, Y. Biomolecule-Assisted Synthesis and Electrochemical Hydrogen Storage of Bi_2S_3 Flowerlike Patterns with Well-Aligned Nanorods. *J. Phys. Chem. B* **2006**, *110*, 8978–8985.
17. Xiong, S.; Xi, B.; Xu, D.; Wang, C.; Feng, X.; Zhou, H.; Qian, Y. L-Cysteine-Assisted Tunable Synthesis of PbS of Various Morphologies. *J. Phys. Chem. C* **2007**, *111*, 16761–16767.
18. Jiang, J. H.; Yu, R. L.; Yi, R.; Qin, W. Q.; Qiu, G. Z.; Liu, X. H. Biomolecule-assisted Synthesis of Flower-like NiS Microcrystals *via* a Hydrothermal Process. *J. Alloys Compd.* **2010**, *493*, 529–534.
19. Chen, L. Y.; Zhang, Z. D. Biomolecule-Assisted Synthesis of $In(OH)_{(3)}$ Hollow Spherical Nanostructures Constructed with Well-Aligned Nanocubes and Their Conversion into C-In_2O_3. *J. Phys. Chem. C* **2008**, *112*, 18798–18803.
20. Chen, L. Y.; Zhang, Y. G.; Wang, W. Z.; Zhang, Z. D. Tunable Synthesis of Various Hierarchical Structures of $In(OH)_{(3)}$ and In_2O_3 Assembled by Nanocubes. *Eur. J. Inorg. Chem.* **2008**, *9*, 1445–1451.
21. Chang, K.; Chen, W. X.; Li, H.; Li, H. Microwave-assisted Synthesis of SnS_2/SnO_2 Composites by L-cysteine and their Electrochemical Performances When Used as Anode Materials of Li-ion Batteries. *Electrochim. Acta* **2011**, *56*, 2856–2861.
22. Xu, Y. X.; Sheng, K. X.; Li, C.; Shi, G. Q. Self-Assembled Graphene Hydrogel *via* a One-Step Hydrothermal Process. *ACS Nano* **2010**, *4*, 4324–4330.
23. Chen, S. Q.; Chen, P.; Wu, M. H.; Pan, D.; Wang, Y. Graphene Supported Sn-Sb@carbon Core-Shell Particles as a Superior Anode for Lithium Ion Batteries. *Electrochem. Commun.* **2010**, *12*, 1302–1306.
24. Li, Y. G.; Wang, H. L.; Xie, L. M.; Liang, Y. Y.; Hong, G. S.; Dai, H. J. *J. Am. Chem. Soc.* **2011**, *133*, 7296−7299.
25. Coleman, J. N.; Lotya, M.; O'Neill, A.; Bergin, S. D.; King, P. J.; Khan, U.; Young, K.; Gaucher, A.; De, S.; Smith, R. J.; *et al.* *Science* **2011**, *331*, 568–571.
26. Li, X. L.; Li, Y. D. MoS_2 Nanostructures: Synthesis and Electrochemical Mg^{2+} Intercalation. *J. Phys. Chem. B* **2004**, *109*, 13893–13900.
27. Sun, Y. Q.; Wu, Q.; Shi, G. Q. Graphene Based New Energy Materials. *Energy Environ. Sci.* **2011**, *4*, 1113–1132.
28. Zhang, Y.; Ren, L. Q.; Wang, S. R.; Marathe, A.; Chaudhuri, J.; Li, G. G. Functionalization of Graphene Sheets through Fullerene Attachment. *J. Mater. Chem.* **2011**, *21*, 5386–5391.
29. Zhao, Y. C.; Zhan, L.; Tian, J. N.; Nie, S. L.; Ning, Z. Enhanced Electrocatalytic Oxidation of Methanol on Pd/polypyrrole-Graphene in Alkaline Medium. *Electrochim. Acta* **2011**, *56*, 1967–1972.
30. Dominko, R.; Arcon, D.; Mrzel, A.; Zorko, A.; Cevc, P.; Venturini, P.; Gaberscek, M.; Remskar, M.; Mihailovic, D. Dichalcogenide Nanotube Electrodes for Li-ion Batteries. *Adv. Mater.* **2002**, *14*, 1531–1534.
31. MiKi, Y.; Nakazato, D.; Ikuta, H.; Uchida, T.; Wakihara, M. Amorphous MoS_2 as the Cathode of Lithium Secondary Batteries. *J. Power Sources* **1995**, *54*, 508–510.
32. Wang, G. X.; Bewlay, S.; Yao, J.; Liu, H. K.; Dou, S. K. Tungsten Disulfide Nanotubes for Lithium Storage. *Electrochem. Solid-State Lett.* **2004**, *7*, A321–A323.
33. Xiao, J.; Choi, D. W.; Cosimbescu, L.; Koech, P.; Liu, J.; Lemmon, J. P. Exfoliated MoS_2 Nanocomposite as an Anode Material for Lithium Ion Batteries. *Chem. Mater.* **2010**, *22*, 4522–4524.
34. Guo, P.; Song, H. H.; Chen, X. H. Electrochemical Performance of Graphene Nanosheets as Anode Material for Lithium-ion Batteries. *Electrochem. Commun.* **2009**, *11*, 1320–1324.
35. Liu, H.; Wang, G. X.; Wang, J. Z.; Wexler, D. Magnetite/Carbon Core-Shell Nanorods as Anode Materials for Lithium-ion Batteries. *Electrochem. Commun.* **2008**, *10*, 1879–1882.
36. Yang, S. B.; Feng, X. L.; Zhi, L. J.; Cao, Q. A.; Maier, J.; Mullen, K. Nanographene-Constructed Hollow Carbon Spheres and Their Favorable Electroactivity with Respect to Lithium Storage. *Adv. Mater.* **2010**, *22*, 838–842.
37. Yang, S. B.; Song, H. H.; Chen, X. H. Electrochemical Performance of Expanded Mesocarbon Microbeads as Anode Material for Lithium-Ion Batteries. *Electrochem. Commun.* **2006**, *8*, 137–142.
38. Hummers, W. S.; Offeman, R. E. Preparation of Graphitic Oxide. *J. Am. Chem. Soc.* **1958**, *80*, 1339–1339.